Two Domains of RD3 Antifreeze Protein Diffuse Independently[†]

Nolan B. Holland,[‡,§] Yoshiyuki Nishimiya,[||] Sakae Tsuda,[||] and Frank D. Sönnichsen*[,‡,⊥]

Department of Physiology and Biophysics, Case Western Reserve University, 10900 Euclid Avenue, Cleveland, Ohio 44106, Department of Chemical and Biomedical Engineering, Cleveland State University, 2121 Euclid Avenue, Cleveland, Ohio 44115, and Institute for Biological Resources and Functions, National Institute of Advanced Industrial Science and Technology (AIST), 2-17-2-1 Tsukisamu-Higashi, Toyohira, Sapporo 062-8517, Japan

Received February 1, 2008; Revised Manuscript Received March 19, 2008

ABSTRACT: Antifreeze proteins (AFPs) make up a class of structurally diverse proteins that help to protect many organisms from freezing temperatures by inhibiting ice crystal growth at temperatures below the colligative freezing point. AFPs are typically small proteins with a relatively flat, slightly hydrophobic binding region that matches the lattice structure of a specific ice crystal plane. The only known two-domain AFP is RD3 from the Antarctic eel pout. It consists of two nearly identical type III domains connected by a nine-residue linker. This protein exhibits higher activity than the single-domain protein at low concentrations. The initial solution structure of RD3 revealed that the domains were aligned so that the binding regions were nearly coplanar, effectively doubling the surface area for binding. A more recent report suggests that the domains may not be aligned in solution but rather diffuse independently. To resolve the issue, we have measured the NMR residual dipolar couplings using alignment media of stretched gels and filamentous phage to determine the relative orientation of the domains. We find that the two domains of RD3 are free to move relative to each other, within the constraint of the flexible nine-residue linker. Our data show that there is no strongly preferred alignment in solution. Furthermore, the flexibility and length of the linker are sufficient to allow the two domains to have their binding faces in the same orientation and coplanar for simultaneous binding to an ice crystal surface.

Antifreeze proteins (AFPs)[1] make up a class of proteins that help to protect organisms from freezing temperatures by binding to ice crystals and inhibiting their growth, effectively lowering the freezing temperature of body fluids. AFPs are structurally diverse proteins but are generally small proteins with a relatively flat, slightly hydrophobic ice-binding region (*1, 2*). The most studied AFPs are derived from fish or insects. They are grouped into types on the basis of their structures: antifreeze glycoproteins, α-helical type I AFPs, C-type lectin homologous type II AFPs, small β-sandwich fold type III AFPs, and the β-helical insect AFPs (*1*). More than 10 years ago, the only known antifreeze protein (AFP) with two domains, RD3, was discovered in the Antarctic eel pout (*Lycodichthys dearbornis*) (*3*). In RD3, an unstructured nine-residue linker connects the two nearly identical type III AFP domains. RD3 is of particular interest because it exhibits an unusually high thermal hysteresis activity at low concentrations (*4*). On the basis of the structure of RD3 determined by nuclear magnetic resonance (NMR), the origin of this increased activity was proposed to be the result of alignment of the domains in a nearly coplanar conformation (Figure 1) (*4*). This presumably

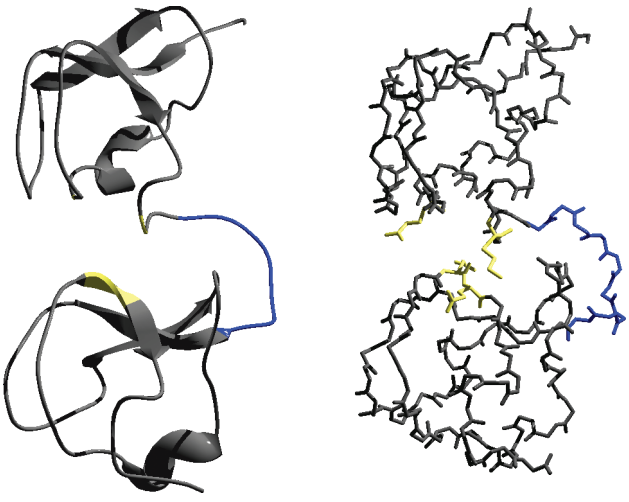

FIGURE 1: Ribbon and stick structures of the two-domain RD3 type III antifreeze protein with the linker colored blue (PDB entry 1C8A). The four interdomain NOE restraints that led to the aligned structure occurred between the residues colored yellow (Q44 and K61 in the N-terminal domain and D122 and Q123 in the C-terminal domain).

[†] This work was supported by the National Institutes of Health (Grants DK07678, GM55326, and DK57306).

* To whom correspondence should be addressed: Department of Physiology and Biophysics, Case Western Reserve University, 10900 Euclid Ave., Cleveland, OH 44106. Telephone: (216) 368-5405. E-mail: fds@case.edu.

[‡] Case Western Reserve University.

[§] Cleveland State University.

[||] National Institute of Advanced Industrial Science and Technology.

[⊥] Current address: Otto Diels Institute for Organic Chemistry, Christian Albrechts University, Otto Hahn Platz 4, 24098 Kiel, Germany. E-mail: fsoennichsen@oc.uni-kiel.de.

[1] Abbreviations: AFP, antifreeze protein; CNS, Crystallography & NMR System; HSQC, heteronuclear single-quantum coherence; IPTG, isopropyl β-D-thiogalactopyranoside; LB, Luria-Bertani; HPLC, high-performance liquid chromatography; NMR, nuclear magnetic resonance; PDB, Protein Data Bank; RDC, residual dipolar coupling; SDS−PAGE, sodium dodecyl sulfate−polyacrylamide gel electrophoresis; TROSY, transverse relaxation optimized spectroscopy.

10.1021/bi8001924 CCC: $40.75
Published on Web 05/07/2008

created one binding region with twice the effective binding area.

We recently reported that substituting glycine for the naturally occurring residues of the linker made the linker significantly more flexible yet did not change the activity of the protein (*5*). Furthermore, residual dipolar coupling measurements on the modified protein suggested that the domains were independently diffusing. These data cast doubts on the validity of the initial structure with prealigned domains and point toward a second proposed mechanism of two independent domains confined to each other by a flexible linker. Without prealignment of the domains, adsorption to ice would occur by the two binding faces independently interacting with the ice surface instead of as a single binding region.

Earlier studies demonstrated that both domains must be functionally active and able to simultaneously bind to the ice surface for full activity (*6*). For this work, two identical type III domains connected with the linker sequence of RD3 were expressed to produce an RD3-like protein with comparable thermal hysteresis behavior. When one of the domains was mutated to make it functionally inactive, the level of thermal hysteresis dropped to a level consistent with an AFP with a non-AFP fusion protein attached. Additionally, when the domains were attached by disulfide bonds such that the two domains were both active, but unable to bind to the same ice crystal surface, the proteins again did not exhibit full activity. These results provide valuable insight but are consistent with the two domains acting as either a prealigned single binding area or two independently binding domains.

Nuclear magnetic resonance (NMR) spectroscopy, in addition to X-ray crystallography, has been a useful tool for the determination of the structure of AFPs. Solution structures are available for all types of AFPs with known structure (*4, 7–12*). NMR also has provided information about the dynamics and solvation of these proteins at temperatures near or even below the freezing point (*12, 13*). A recent development in NMR is the use of residual dipolar coupling (RDC) measurements as constraints on the relative bond angles in proteins, independent of proximity (*14*). RDC values can be obtained by disturbing the isotropic tumbling of the protein using any of a variety of alignment media. RDC restraints have proven to be particularly useful for determining relative orientations of domains in proteins (*15*). In a recent study, RDC measurements were used to establish the independence of domains (*16*).

In this paper, we revisit the original structure calculation of the RD3 and incorporate residual dipolar coupling restraints to determine the domain orientation. These data demonstrate that the domains do diffuse independently, that there is no significant prealignment of the domains, and that both domains can potentially bind to an ice crystal plane with the same orientation.

EXPERIMENTAL PROCEDURES

Protein Expression. ^{15}N-labeled RD3 antifreeze protein was overexpressed in *Escherichia coli* strain BL21(DE3) and purified on the basis of a previously reported protocol (*5*). Bacteria containing the pET 20b plasmid encoding the RD3 gene were grown at 20 °C in 1 L of LB medium supplemented with ampicillin (100 μM) until the cell growth reached the early stationary phase ($OD_{600} \sim 0.6$). The cells were collected by centrifugation at 4000*g* for 30 min at 4 °C followed by resuspension in 1 L of M9 minimal medium containing [^{15}N]ammonium chloride. After equilibration at 37 °C on an orbital shaker at 200 rpm , the expression of RD3 was induced by addition of 0.5 mM IPTG. After 6 h, the culture was removed from the shaker and centrifuged at 4000*g* for 30 min at 4 °C. The precipitated cell pellet was lysed using B-PER reagent (Pierce), including lysozyme. Most of the RD3 was contained in inclusion bodies, which were collected in the insoluble fraction by centrifugation at 27000*g* for 15 min. The pellet was washed several times in B-PER diluted 20:1 with water followed by centrifugation. The pellet was dissolved in 10 mL of 6 M guanidine hydrochloride. Buffer and water were added to the protein solution to yield a 200 mL solution with 50 mM potassium phosphate and 100 mM sodium chloride (pH 10.7). The protein solution was kept for at least 2 days at 4 °C. The solution was then extensively dialyzed in a 1 kDa molecular mass cutoff tube against a solution of 50 mM acetic acid and ammonium bicarbonate (pH 3.7), with a final dialysis against dilute acetic acid (pH 3.7). The precipitate was removed by centrifugation, and the supernatant containing nearly pure RD3 (>95%) was lyophilized. The yield ranged from 125 to 170 mg/L of culture. Higher purity could be achieved using reverse phase HPLC (*4*) but was unnecessary for the NMR experiments. SDS−PAGE was used to follow the entire process of expression and purification. Samples for NMR (7.3 mg/mL, 0.5 mM) were prepared in 50 mM potassium chloride and 2 mM sodium azide solutions containing 10% D_2O at pH 6.8.

Alignment for RDC Measurement. Three independent weak alignments of RD3 for RDC measurements were obtained using two different media: filamentous phage (*17*) and stretched acrylamide gels (*18*).

For phage alignment, three aliquots of 25 μL of 51 mg/mL Pf1 filamentous phage solution (Profos, Regensburg, Germany) were added to 200 μL of the NMR protein solution in a Shigemi NMR tube, resulting in a final concentrations of 14 mg/mL for phage and 5.3 mg/mL for RD3. ^{15}N HSQC spectra were obtained after each aliquot to ensure that the phage did not significantly affect the spectral quality.

Stretched acrylamide gels were prepared from 7% acrylamide (60:1 acrylamide:bisacrylamide ratio) in 50 mM KCl solutions. Ammonium persulfate (0.08%) and TEMED (0.7%) were added, and following brief mixing, the solutions were pipetted into tubes with an inside diameter of 4.70 mm, 1.36 times greater than that of the NMR tube. After setting, the gels were extracted, cut to 2.9 cm lengths (500 μL volume), and soaked for several hours in an excess of purified water (18.2 MΩ cm) to remove salts and unreacted acrylamide. The gels were then dried under ambient conditions overnight. The dry gels were swelled to their original size in 500 μL of NMR protein solution described above. The protein-containing gels were squeezed into an open-ended 4.24 mm Wilmad NMR tube using a home-built plunger system, based on the design of Chou et al. (*19*). The resulting gel was elongated by symmetric radial compression to a length of 3.5 cm.

A third independent alignment was obtained by using an asymmetric stretching of a gel. The gels were prepared identically as described above but, instead of being cast in

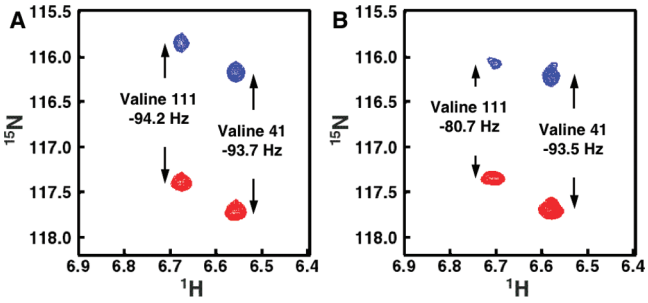

FIGURE 2: Overlays of the TROSY (^{15}N downfield, red) and the ^{15}N upfield multiplet (blue) components of RD3 (A) in solution and (B) aligned in a stretched acrylamide gel. The difference in the peak positions in the solution data provides the values for *J* coupling, while the gel sample provides the *J* coupling and the residual dipolar coupling (RDC) values. RDCs for each of the N−H bonds in the backbone were measured.

a round tube, were cast in tubes with an oval cross section prepared by flattening a serological pipet. The minor axis was the same size as the inner diameter of an NMR tube, while the major axis was twice as large. When this gel was squeezed into the NMR tube, stretching of the gel was not radially symmetric. This approach is analogous to obtaining different alignments by confining aligned phage in a gel and placing it in the magnetic field at a different angle (*20*).

RDC Measurement. RDC measurements were taken from NMR spectra obtained with a 600 MHz Varian INOVA spectrometer at 4 °C. On the basis of the pulse sequences reported by Weigelt (*21*), two TROSY-type experiments were performed each selecting a different ^{1}H upfield component of the ^{1}H−^{15}N multiplet. ^{1}H−^{15}N coupling was obtained from the difference between the peak positions in the standard TROSY (^{15}N downfield) and ^{15}N upfield spectra. These couplings were measured for each of the partially aligned samples and for an unaligned solution. In each case, the two corresponding spectra were obtained sequentially using identical spectrometer parameters except for the number of transients [180 increments of 512 complex points, spectral widths of 6600 Hz (^{1}H) and 1650 Hz (^{15}N)]. Because of broader peaks, the ^{15}N upfield spectra required more transients to produce signal-to-noise ratios at the same level as in the TROSY spectra.

NMRPipe (*22*) was used to process the spectra, and NMRView (*23*) was used for spectral analysis. HSQC peak positions from the reported assignments of RD3 were translated by the expected *J* coupling values for each different spectrum. These estimated peak positions were used to identify the TROSY and ^{15}N upfield spectra. Because of the significant overlap of peaks (since the two domains have nearly identical structures), not all peaks could be assigned unambiguously, particularly in spectra from aligned media where the coupling deviated from typical *J* coupling values. For all of the unambiguously identified peaks, the ^{1}H−^{15}N coupling was measured for the three aligned samples and the unaligned sample. The residual dipolar couplings were determined as the differences in couplings between the aligned and unaligned samples. It is important to note that if the aligned samples resulted in peaks that were closer together than the unaligned sample, the sign of the RDC is positive, since the ^{1}H−^{15}N *J* coupling has a negative value (Figure 2).

Determination of RDC Parameters. Measured RDC values, δ, are converted to bond angle restraints in polar coordinates, based on the following relationship (*24*):

$$\delta(\Theta, \varphi) = \frac{3}{2}\delta_{\max}\left[\frac{1}{2}(3\cos^2\Theta - 1)A_{zz} + \frac{1}{2}\sin^2\Theta\cos 2\varphi \times (A_{xx} - A_{yy})\right] \quad (1)$$

where Θ is the angle between the bond and *z*-axis, φ is the angle of the bond projected onto the $x-y$ plane, and A_{ii} is the relative alignment to the *i* axis. If the axial and rhombic components of the alignment tensors are defined (*17*), the equation simplifies to

$$\delta(\Theta, \varphi) = D_a(3\cos^2\Theta - 1) + \frac{3}{2}D_r\sin^2\Theta\cos 2\varphi \quad (2)$$

where $D_a = {}^3/_4\delta_{\max}A_{zz}$ and $D_r = {}^1/_2\delta_{\max}(A_{xx} - A_{yy})$. Within CNS, the alignment tensor is defined by the parameters D_a and $R = D_r/D_a = {}^2/_3(A_{xx} - A_{yy})/A_{zz}$.

PALES (*25*) was used to establish preliminary alignment coefficients (D_a and D_r) for the residual dipolar couplings and to establish that the RDCs fit to the structures that were calculated. The quality of the fit in PALES indicates the compatibility of the structures to the RDC values.

Structure Calculations. Structure calculations for RD3 were performed using CNS 1.1 (*26*). In addition to the structural restraints used for the two domains in the former structure calculations (*27*), which consisted of 1476 NOEs, 80 H-bond restraints, and 80 dihedral restraints, RDC restraints measured here were added as additional experimental restraints. RDCs were grouped for each domain and restrained to two independent alignment tensors. Tensor coefficients were determined for each domain individually, by systematic variation of initial estimates for the D_a and R values derived from PALES analysis, using the minimized average structure for RD3 (PDB entry 1C8A). Structure calculations employed random velocity assignments, a time step of 5 fs, high-temperature Cartesian dynamics at 1000 K for 10000 steps, a cooling stage of Cartesian dynamics for 50000 steps, and 200 steps of minimization. During the annealing step, internal force constants were rescaled following the standard CNS annealing protocol. Calculations were repeated until a set of 200 structures without violations of experimental restraints (<0.3 Å NOE, <5° dihedral angles, and 1.5 Hz for RDCs) was obtained.

RESULTS

Residual dipolar coupling measurements of RD3 were taken successfully with three different alignments. The RDCs for each case were sufficiently large to obtain a reasonable distribution, and a minimum of 24 was obtained in each domain. For each of the alignments, the distributions of the RDC values appear to differ for the two domains (Figure 3).

PALES was used to determine if the RDC values were consistent with the previously reported structure (PDB entry 1C8A) (*4*). Using any full set of RDC values (i.e., from both domains) shows a poor fit to the 1C8A structure as determined by the error values. However, if RDC values from only one of the two domains are used, they fit well to the structure. Therefore, the reported domain structures are

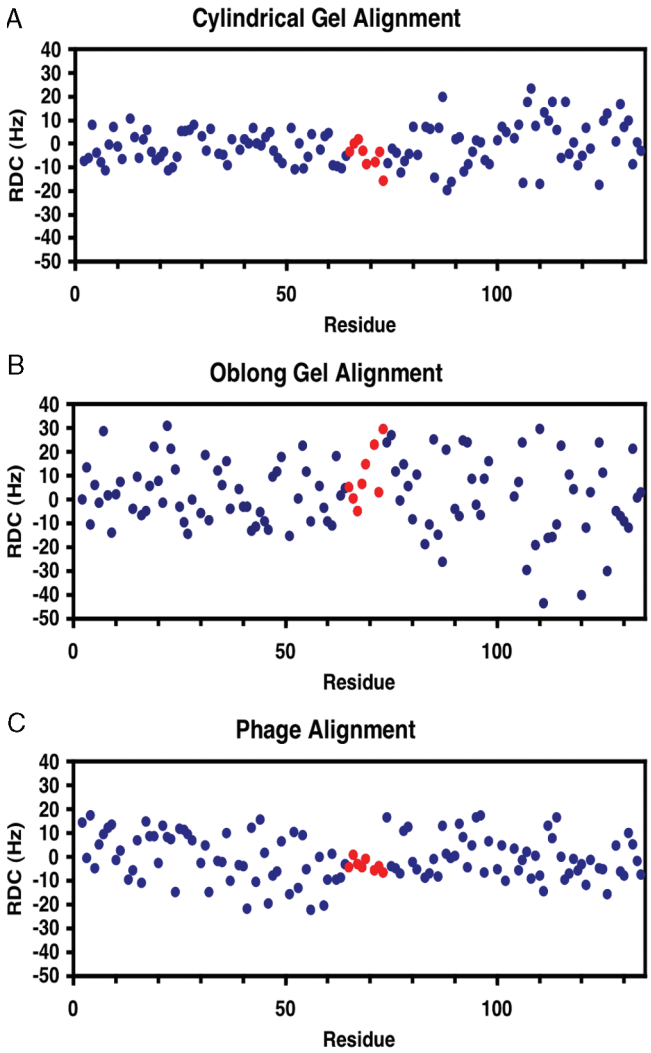

FIGURE 3: RDC values for the RD3 aligned by acrylamide gel (A, symmetrical; B, oblong) and Pf1 filamentous phage (C). The distributions of the RDCs for the two domains are clearly different for each alignment. The different distributions indicate that the domains diffuse independently and so have different degrees of alignment. Further, these RDC values define a specific range of angles in which the bond lies with respect to the molecular axis. Using the RDC values, the relative orientation of the aligned domains can be determined.

consistent with our measurements, but the orientation of the domains in 1C8A is different from that of our aligned samples.

We then used structure calculations incorporating the RDC values as restraints to determine the aligned structure of RD3. To do this, the restraints that led to the domain alignment in 1C8A had to be removed to allow free alignment of the domains. Upon inspection, only four interdomain NOE restraints were found (Figure 1). In structures calculated without these restraints, the domains were no longer aligned (Figure 4). When one domain is overlaid, the second domain is shown to be able to access a large range of space apparently only constrained by the reach of the flexible linker and the prohibition of domain overlap.

RDCs from the phage alignment were added to the restraint file with the interdomain NOE restraints removed. To maximize the fitting of the RDCs, different D_a and R values were used for each domain (Table 1). A poor fit resulted if a single set of parameters was used. This is

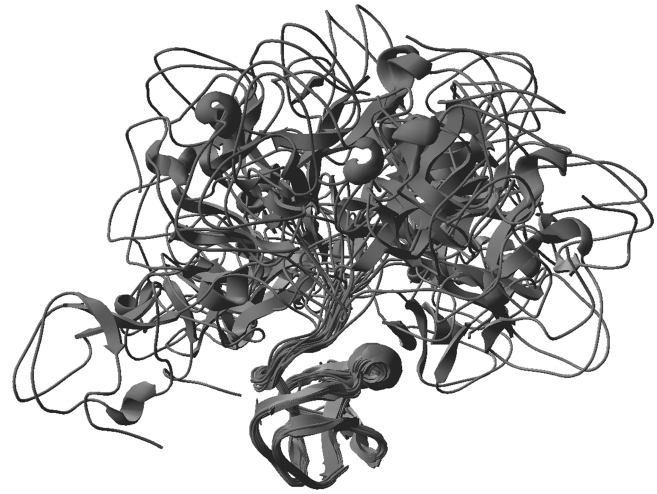

FIGURE 4: Ensemble of 25 structures of RD3 calculated with independent alignment axes. This gives a representation of the possible conformations of an unaligned RD3 in solution. The domain orientation is restricted only by the flexibility of the linker and the steric interaction of the domains. Overlaying the N-terminal domains illustrates the range of orientations that are accessible.

Table 1: Alignment Constants for the Different Alignment Media

	N-domain		C-domain	
alignment medium	D_a	R	D_a	R
symmetric stretched gel	8.5	0.85	12.4	0.36
asymmetric stretched gel	16.4	0.86	20.0	0.35
Pf1 filamentous phage	11.0	0.40	7.0	1.10

consistent with the fact that the RDC distributions are different for the two domains, indicating the presence of an independent alignment. The calculations resulted in well-folded structures. When one domain of these structures is overlaid, four different sets of structures are observed (Figure 5C). It should be noted that only one of those sets represents the actual average domain alignment, while the other three are mathematical equivalents in which the second domain is rotated by 180° around the *x*-, *y*-, or *z*-axis.

Using additional alignment media with differing alignment axes adds additional information that can help distinguish the real structure from the symmetry-related structures. The calculated structures should consist of the same actual structure, but the mathematical equivalents are the result of rotations about a different set of axes. Thus, only the real structure will be present in both sets of structures and can be identified by overlaying the resulting data sets. To this end, two more structure calculations were performed with the set of RDCs from the stretched gel and from the asymmetric stretched gel (Figure 5A,B). The results of this were somewhat surprising. As expected, there was one structure common to the stretched gel and the asymmetric stretched gel (Figure 6); however, there was no common structure between the phage alignment and either of the stretched gels.

DISCUSSION

The principal goal of this study was to determine the relationship between the two domains of the RD3 antifreeze protein by using residual dipolar coupling measurements as additional restraints. We recently reported that RD3 with a more flexible linker retained the same activity as the native

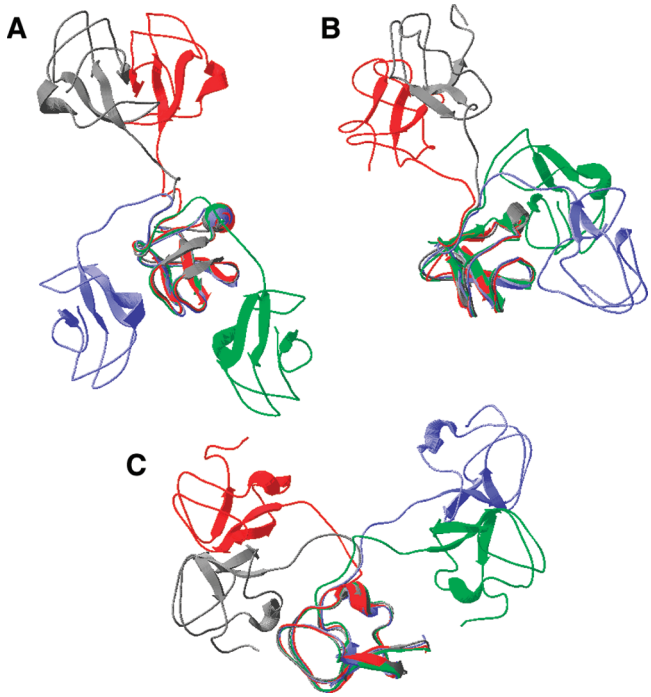

FIGURE 5: Ensembles of RD3 structures with overlaid N-terminal domains calculated with a single alignment axis for each domain: cylindrical gel alignment (A), oblong gel alignment (B), and phage alignment (C). These ensembles can be reduced to four sets of unique domain orientations for each alignment as illustrated by the four backbone traces. Only one is the actual structure, while the other three represent mathematically equivalent orientations which are 180° rotations of the domain about the *x*-, *y*-, and *z*-axes.

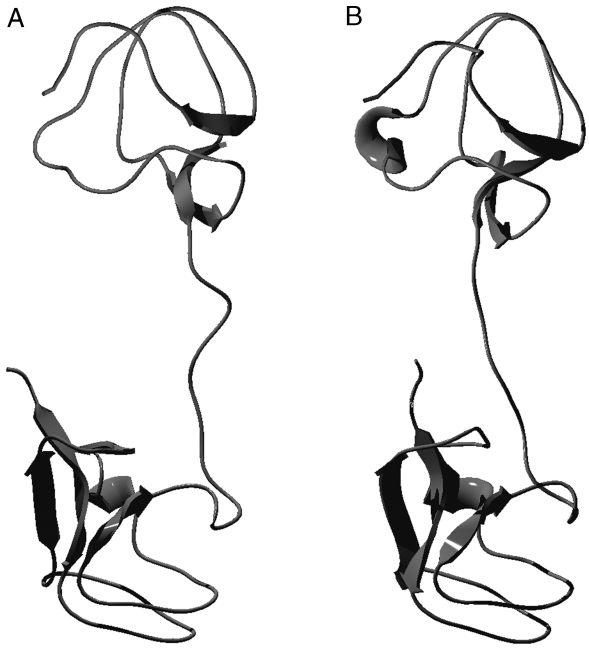

FIGURE 6: Common structure for the oblong (A) and cylindrical (B) gel alignment media. This is the only orientation that is common between the two sets of orientations. This common structure is the actual aligned orientation of RD3 in the acrylamide gel. Neither this orientation nor any of the others match any of the phage-aligned orientations. This indicates that the protein has a different alignment by the phage.

protein (*5*). We also found that the two domains had different RDC distributions, indicating diffusional independence of the two domains. To confirm this, we successfully measured RDCs with three different alignments and calculated structures for each. The results lead to the conclusion that in solution, the domains of RD3 diffuse independently, as opposed to being prealigned as previously reported.

Our data show that alignment with a stretched gel, whether symmetric or asymmetric, results in one orientation of the domains. This domain orientation is different from the originally published structure (*4*) and also is different from the possible structures determined by phage alignment. The different conformations measured in different media indicate that if there is some preferred alignment of the domains in solution, it is weak and easily perturbed by the environment.

By reaching this conclusion, we think it is important to discuss why the original structure determination indicated a domain prealignment. This alignment in the original structure was dependent on only four interdomain NOEs, which were assigned between charged side chains, one in each domain. When structure calculations were carried out here with these four restraints removed, the domains were no longer aligned (similar to Figure 4). Since the measured RDC data did not fit the original aligned structure, it was necessary to remove the interdomain NOEs in this study to determine the domain orientations in the aligned media. This indicates that these NOEs do not accurately reflect the structure of the protein in different alignment media. There are several possibilities with respect as to the origin of these NOEs. It is possible that the original alignment is a weakly preferred solution orientation and that this structure has a higher probability of occurring than other domain orientations, leading to the observed NOEs. In the alignment media, this orientation is disturbed, leading to a different domain orientation. Alternatively, the NOE observations could be transient NOEs that are observed as the domains come temporarily into the proximity of each other from the free movement of the domains. In either case, NOE averaging would result in distance restraints smaller than the actual average atomic separation. It could also be the result of a mistaken assignment for the NOEs. In fact, if the original structure were correct, one expects to see many more NOEs from atoms that are in the proximity of each other. This leads us to believe the latter scenario is more probable. In any case, these NOEs are not consistent with the large set of measured RDCs and need to be excluded from the structure calculations.

The difference in the structures determined for phage alignment and gel alignment is due to the nature of the alignment. The stretched gel aligns protein principally through steric interactions. There is little chemical interaction between the acrylamide gel and the protein. This leads the protein to be aligned primarily by its shape, with the longest axis aligning with the extended direction of the gel, in our case with the *z*-axis. For two domains linked by a flexible linker, one would expect the two domains to align with the gel, and then the individual domains would orient on the basis of their geometry. Since the linker is attached to the carboxy terminus in one domain and amino terminus of the other, there is asymmetry in the shape of the domains relative to the linker position. This is the origin of the different alignment constants for the two domains. In essence, the domains are first confined to an orientation based on the other domain, but the individual domains now have limited flexibility to align on the basis of the domain geometry. Notably, a common domain orientation was found for the

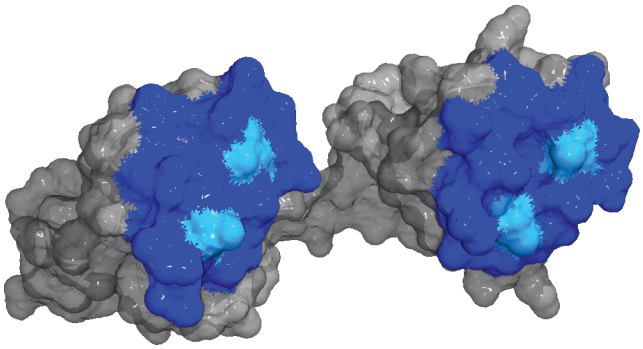

FIGURE 7: One of the four structures from phage alignment with similar domain orientations. The view shows the binding faces with residues T15 and T18 of the first domain and the corresponding residues T85 and T88 of the second domain highlighted. Since the phage aligns through electrostatic interactions, it would be expected that the two domains would have a similar alignment. On the basis of this, we suggest that this structure represents the most likely actual orientation of the domains. Given the demonstrated flexibility of the linker, this structure also illustrates the possibility of simultaneous binding of the two domains to an ice surface with the same orientation.

two different stretched gels since the alignment mechanism is the same.

The phage alignment works through a different mechanism. It relies less on steric alignment and more on chemical interactions with the phage, namely electrostatic interactions. Since this is the case, the direction of the one domain relative to the other is less important. The alignment of the domains should principally be based on the electrostatic characteristics of the domains. Since the domains are nearly identical, the alignment should orient the domains in the same orientation. If we look at the four possible domain orientations for the structures calculated from the phage RDCs, we find that one has the domains in nearly the same orientation (Figure 7). We propose that this is the actual alignment in the phage solution. It is interesting to note that this alignment would be the orientation needed for both domains to bind to the ice surface simultaneously with the same orientation to the ice plane. It would not be necessary for the binding face to interact with an ice plane in different orientations.

The main consequence of the finding that the domains diffuse independently will be in the theoretical treatment of the origin of the increased activity of RD3. Kristiansen and Zachariassen presented a mechanism for thermal hysteresis activity by describing AFP interacting with an ice surface with equilibrium exchange at the melting temperature, followed by irreversible adsorption at temperatures below the melting point (*28*). This model reconciles the need for irreversible binding to explain the ice growth inhibition with the observed concentration dependence of thermal hysteresis. The reversible equilibrium adsorption at the melting temperature explains the concentration dependence of thermal hysteresis, while the irreversible adsorption at lower temperatures allows for the complete inhibition of crystal growth.

For our system, we are interested in characterizing the concentration dependence of the thermal hysteresis and so consider the reversible adsorption aspect of the model. The original proposed structure of RD3 with prealigned domains that bind to the ice as a single unit suggests that the binding area is doubled, increasing the affinity for the surface. This is equivalent to additional repeats in the helical-type antifreeze proteins such as type I fish AFP (*29–31*) and insect AFP (*32, 33*). However, if the domains bind independently, as we propose, the affinity of the individual domains remains the same as that of the single-domain proteins. The difference is, however, that for the entire protein to desorb, both domains must detach from the surface. The relative rates of desorption and adsorption of the individual domains will dictate the probability of the entire protein desorbing. In effect, this is an increase in the avidity of the protein for the ice surface. It is expected to result in increased adsorption particularly at low concentrations, while the effect is weaker as the protein concentration increases, consistent with the observed activity of RD3 in thermal hysteresis measurements (*4*).

We conclude that the two stably folded type III domains of RD3 are free to move relative to each other, within the constraint of the flexible nine-residue linker. We find it inconsistent with our data that there is any strongly preferred alignment in solution, which was previously reported (*4*). Furthermore, the flexibility and length of the linker are sufficient to allow the two domains to have their binding faces in the same orientation and coplanar for simultaneous binding to an ice crystal surface.

ACKNOWLEDGMENT

We thank Drs. Dale Ray and Xian Mao for spectrometer maintenance and the Cleveland Center for Structural Biology for use of their NMR facilities.

REFERENCES

1. Davies, P. L., Baardsnes, J., Kuiper, M. J., and Walker, V. K. (2002) Structure and function of antifreeze proteins. *Philos. Trans. R. Soc. London, Ser. B 357*, 927–933.
2. Sönnichsen, F. D., DeLuca, C. I., Davies, P. L., and Sykes, B. D. (1996) Refined solution structure of type III antifreeze protein: Hydrophobic groups may be involved in the energetics of the protein-ice interaction. *Structure 4*, 1325–1337.
3. Wang, X., Devries, A. L., and Cheng, C. H. C. (1995) Antifreeze peptide heterogeneity in an antarctic eel pout includes an unusually large major variant comprised of 2.7-KDa Type-III AFPs linked in tandem. *Biochim. Biophys. Acta 1247*, 163–172.
4. Miura, K., Ohgiya, S., Hoshino, T., Nemoto, N., Suetake, T., Miura, A., Spyracopoulos, L., Kondo, H., and Tsuda, S. (2001) NMR analysis of type III antifreeze protein intramolecular dimer: Structural basis for enhanced activity. *J. Biol. Chem. 276*, 1304–1310.
5. Holland, N. B., Nishimiya, Y., Tsuda, S., and Sönnichsen, F. D. (2007) Activity of a two-domain antifreeze protein is not dependent on linker sequence. *Biophys. J. 92*, 541–561.
6. Baardsnes, J., Kuiper, M. J., and Davies, P. L. (2003) Antifreeze protein dimer: When two ice-binding faces are better than one. *J. Biol. Chem. 278*, 38942–38947.
7. Graether, S. P., Kuiper, M. J., Gagne, S. M., Walker, V. K., Jia, Z. C., Sykes, B. D., and Davies, P. L. (2000) β-Helix structure and ice-binding properties of a hyperactive antifreeze protein from an insect. *Nature 406*, 325–328.
8. Liepinsh, E., Otting, G., Harding, M. M., Ward, L. G., Mackay, J. P., and Haymet, A. D. J. (2002) Solution structure of a hydrophobic analogue of the winter flounder antifreeze protein. *Eur. J. Biochem. 269*, 1259–1266.
9. Kwan, A. H. Y., Fairley, K., Anderberg, P. I., Liew, C. W., Harding, M. M., and Mackay, J. P. (2005) Solution structure of a recombinant type I sculpin antifreeze protein. *Biochemistry 44*, 1980–1988.
10. Sönnichsen, F. D., Sykes, B. D., Chao, H., and Davies, P. L. (1993) The non-helical structure of antifreeze protein type-III. *Science 259*, 1154–1157.
11. Gronwald, W., Loewen, M. C., Lix, B., Daugulis, A. J., Sönnichsen, F. D., Davies, P. L., and Sykes, B. D. (1998) The solution structure

of type II antifreeze protein reveals a new member of the lectin family. *Biochemistry 37*, 4712–4721.
12. Daley, M. E., Spyracopoulos, L., Jia, Z. H., Davies, P. L., and Sykes, B. D. (2002) Structure and dynamics of β-helical antifreeze protein. *Biochemistry 41*, 5515–5525.
13. Gronwald, W., Chao, H. M., Reddy, D. V., Davies, P. L., Sykes, B. D., and Sönnichsen, F. D. (1996) NMR characterization of side chain flexibility and backbone structure in the type I antifreeze protein at near freezing temperatures. *Biochemistry 35*, 16698–16704.
14. Tolman, J. R., Flanagan, J. M., Kennedy, M. A., and Prestegard, J. H. (1995) Nuclear magnetic dipole interactions in field-oriented proteins: Information for structure determination in solution. *Proc. Natl. Acad. Sci. U.S.A. 92*, 9279–9283.
15. Fischer, M. W. F., Losonczi, J. A., Weaver, J. L., and Prestegard, J. H. (1999) Domain orientation and dynamics in multidomain proteins from residual dipolar couplings. *Biochemistry 38*, 9013–9022.
16. Poon, D. K. Y., Withers, S. G., and McIntosh, L. P. (2007) Direct demonstration of the flexibility of the glycosylated proline-threonine linker in the *Cellulomonas fimi* xylanase Cex through NMR spectroscopic analysis. *J. Biol. Chem. 282*, 2091–2100.
17. Clore, G. M., and Gronenborn, A. M. (1998) New methods of structure refinement for macromolecular structure determination by NMR. *Proc. Natl. Acad. Sci. U.S.A. 95*, 5891–5898.
18. Tycko, R., Blanco, F. J., and Ishii, Y. (2000) Alignment of biopolymers in strained gels: A new way to create detectable dipole-dipole couplings in high-resolution biomolecular NMR. *J. Am. Chem. Soc. 122*, 9340–9341.
19. Chou, J. J., Gaemers, S., Howder, B., Louis, J. M., and Bax, A. (2001) A simple apparatus for generating stretched polyacrylamide gels, yielding uniform alignment of proteins and detergent micelles. *J. Biomol. NMR 21*, 377–382.
20. Trempe, J. F., Morin, F. G., Xia, Z. C., Marchessault, R. H., and Gehring, K. (2002) Characterization of polyacrylamide-stabilized Pf1 phage liquid crystals for protein NMR spectroscopy. *J. Biomol. NMR 22*, 83–87.
21. Weigelt, J. (1998) Single scan, sensitivity- and gradient-enhanced TROSY for multidimensional NMR experiments. *J. Am. Chem. Soc. 120*, 10778–10779.
22. Delaglio, F., Grzesiek, S., Vuister, G. W., Zhu, G., Pfeifer, J., and Bax, A. (1995) NMRPipe: A multidimensional spectral processing system based on Unix pipes. *J. Biomol. NMR 6*, 277–293.
23. Johnson, B. A., and Blevins, R. A. (1994) NMR View: A computer program for the visualization and analysis of NMR data. *J. Biomol. NMR 4*, 603–614.
24. Bax, A., Kontaxis, G., and Tjandra, N. (2001) Dipolar couplings in macromolecular structure determination. *Methods Enzymol. 339* (Part B), 127–174.
25. Zweckstetter, M., and Bax, A. (2000) Prediction of sterically induced alignment in a dilute liquid crystalline phase: Aid to protein structure determination by NMR. *J. Am. Chem. Soc. 122*, 3791–3792.
26. Brünger, A. T., Adams, P. D., Clore, G. M., DeLano, W. L., Gros, P., Grosse-Kunstleve, R. W., Jiang, J. S., Kuszewski, J., Nilges, M., Pannu, N. S., Read, R. J., Rice, L. M., Simonson, T., and Warren, G. L. (1998) Crystallography & NMR system: A new software suite for macromolecular structure determination. *Acta Crystallogr. D54*, 905–921.
27. Miura, K., Ohgiya, S., Hoshino, T., Nemoto, N., Nitta, K., and Tsuda, S. (2000) Assignments of H-1, C-13, and N-15 resonances of intramolecular dimer antifreeze protein RD3. *J. Biomol. NMR 16*, 273–274.
28. Kristiansen, E., and Zachariassen, K. E. (2005) The mechanism by which fish antifreeze proteins cause thermal hysteresis. *Cryobiology 51*, 262–280.
29. Chao, H., Hodges, R. S., Kay, C. M., Gauthier, S. Y., and Davies, P. L. (1996) A natural variant of type I antifreeze protein with four ice-binding repeats is a particularly potent antifreeze. *Protein Sci. 5*, 1150–1156.
30. Harding, M. M., Ward, L. G., and Haymet, A. D. J. (1999) Type I 'antifreeze' proteins: Structure-activity studies and mechanisms of ice growth inhibition. *Eur. J. Biochem. 264*, 653–665.
31. Houston, M. E., Chao, H., Hodges, R. S., Sykes, B. D., Kay, C. M., Sönnichsen, F. D., Loewen, M. C., and Davies, P. L. (1998) Binding of an oligopeptide to a specific plane of ice. *J. Biol. Chem. 273*, 11714–11718.
32. Leinala, E. K., Davies, P. L., Doucet, D., Tyshenko, M. G., Walker, V. K., and Jia, Z. C. (2002) A β-helical antifreeze protein isoform with increased activity: Structural and functional insights. *J. Biol. Chem. 277*, 33349–33352.
33. Marshall, C. B., Daley, M. E., Sykes, B. D., and Davies, P. L. (2004) Enhancing the activity of a β-helical antifreeze protein by the engineered addition of coils. *Biochemistry 43*, 11637–11646.

BI8001924